



Università degli Studi di Napoli Federico II

Scuola Politecnica e delle Scienze di Base

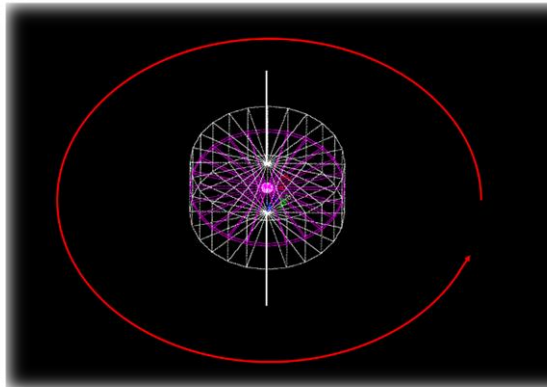
Collegio di Scienze

Dipartimento di Fisica "Ettore Pancini"

Corso di Laurea Magistrale in Fisica

TESI DI LAUREA SPERIMENTALE IN FISICA MEDICA

A new technique for rotational radiotherapy of breast cancer with synchrotron radiation microbeam.



Relatore

Prof. Paolo Russo

Prof. Giovanni Mettivier

Dott. Antonio Sarno

Candidata

Dott.ssa Valentina Pirozzi Palmese

Matr. N94/351

*Non sono le nostre capacità a definire ciò che siamo
ma le nostre scelte. (cit.)
Al mio papà e alla mia mamma,
non smettete mai di lottare.*

A new technique for rotational radiotherapy of breast cancer with synchrotron radiation microbeam.

Table of Contents

Introduction.....	5
Chapter 1: Microbeams RadioTherapy (MRT).....	8
1.1. Peak to valley dose.....	10
1.2. Radiobiology point of view.....	14
Chapter 2: Simulations.....	20
2.1. Geant4 code.....	20
2.2. Simulation set-up.....	21
2.3. Collimator.....	23
2.4. Single projection.....	24
2.4.1. Micro source project.....	24
2.4.2. Single beamlet.....	27
2.4.3. Multi beamlets.....	29
2.5. Rotated microbeam.....	31
2.5.1. Different rotational axis.....	37
2.6. Study of the vertical divergence beam.....	39
Chapter 3: Dose measurements.....	43
3.1. MRT measures via EBT3.....	44
Conclusion.....	51
Bibliography.....	53
Acknowledgements.....	55

Introduction

The breast cancer is the most common malignancy in the woman ^[1]. Standard care protocols included Radiation Therapy (RT), after breast-conserving surgery to remove any residual cancer cells in order to reduce the risk of relapse or in case of intermediate or high risk of loco regional failure after mastectomy.

However, it has some limitation related to the dose off-target deposited in the other organs, for example heart and lungs.

Microbeam Radiation Therapy (MRT) is an innovative experimental technique potentially able to overcome this limitation. It combines most tolerance for normal tissue at dose of several hundred Gy, instead, in most clinical radiotherapy schedules single fraction doses are between 1.5 Gy and 3 Gy, with the high collimation and dose rate of synchrotron light.

Indeed, radiation therapy using synchrotron-generated X-rays makes a significant contribution to improve radiation therapy, also for breast cancer, as show the study on the Synchrotron Radiation Rotational RadioTherapy (SR³T) ^[2].

Pre-clinical MRT studies have been designed to replace an entire conventional radiotherapy schedule with one single treatment session of MRT, similar to the approach already established for clinical radiosurgery or integrated MRT as boost into a conventional radiotherapy schedule, take advantage of the possibility to deliver a very high dose compared to the conventional therapy ^[3].

At the state of art, there are three oncological targets could profit from MRT: malignant brain tumours, lung cancer and malignant tumours of the musculoskeletal system.

For the first time the medical physics group in Napoli, investigated the possible future development of the MRT techniques for the breast cancer, inside the project SR³T, with the purpose to find a better deal between the efficiency of the treatment in term of remove the tumour and save dose to normal tissue along the path.

Today few places have a synchrotron facility, because it needs many investments, space and highly qualified staff. But the positive result of its use for the medical scope and the rapid developed of new technology make to possible create a hospital infrastructure accessible to the irradiation hutch of such a wiggler is a challenge that should not be underestimated, but analogous challenges of comparable difficulty have been overcome. In my work, I implemented the Geant4 application developed by Dr Antonio Sarno, to study the feasibility of the MRT technique for the treatment of breast cancer in planar or circular geometry.

We simulated the monoenergetic irradiation on cylindrical phantom in order to evaluate the Peak to Valley Dose Ratio (PVDR) in a projection irradiation, and the 3D dose distribution in a partial or fully tomographic irradiation. The cylindrical phantom of 14 cm diameter simulated the pendant breast of the patient in prone position. The source was a rectangular parallel monochromatic beam in the energy range from 50 to 150 keV, passing through a tungsten comb collimator (4 mm thick) with slit width 50 μm and slits separation of 500 μm centre-to-centre.

Chapter 1 presents a short overview of the various aspect of MRT, the starter idea, the most important dosimetric parameters, the principal radiobiological hypotheses and studies result found in the last year.

Chapter 2 contains the heart of my thesis work. The simulation results in term of the dose distribution in a cylinder phantom that simulate the pendent breast.

I looked for 3D dose distribution in different material, the effect of presence of a “physical” collimator, the shape of the source, its divergence and dynamic like circular orbit.

At the end, in chapter 3, I compared the simulation results with the dosimetric measurement by EBT3 GafChromic™, conducted at the BMIT-ID beamline of the Canadian Light Source.

Chapter 1: Microbeams RadioTherapy (MRT)

The usefulness of radiation therapy for tumours rely suppress the clonogenicity of most neoplastic cells in a tumour, with doses restricted to safe limits. The highest goal of each techniques is to optimize dose distributions, in order to damage the target and preserve the normal tissue around and the path of the radiation.

Especially when tumors are large, irregularly shaped, deep-seated and near one or more radiosensitive organs. The most widely available radiation sources for such cases are electron linear accelerators with sophisticated treatment-planning software and beam delivery systems. Treatment planning can be relatively straightforward, shaping a beam of 4–11MeV photons by physical or electronic wedges and using collimators fabricated for the individual patient, or computer-controlled multi-leaf collimators (MLC). It is possible to perform conformal radiotherapy by moving a beam in an arc around the target.

Archive protection of sensitive normal tissues by modulating the intensity and the shape of the beam. The resultant is high-dose treatment volume shaped to comprise the zone of macroscopic tumor and a peripheral shell of presumed microscopic tumor invasion. This margin can be overcome for setup error and possible movement of the target during irradiation. Furthermore, an intrinsic limitation for photons is the exponential fall-off of dose with depth, that limiting doses proximal and distal to such targets ^[5].

Microbeam irradiation is spatially fractionated radiation on a micrometer scale, its use as therapeutic intent has become known as microbeam radiation therapy (MRT), it allows to spare skin entrance doses compared to the target dose for every single beam.

The idea was born in the late 1950s, during a study of effect of the cosmic radiation to astronauts, by the collaboration between the biophysicist Howard J. Curtis and the atomic physicist Charles P. Baker at the Brookhaven National Laboratory (BNL).

They used a deuteron microbeam to irradiate mice, in order to simulate the damage in the human brain caused by energetic cosmic rays during space exploration programs and observed that normal brain tissue tolerance is very high if it is irradiated with 25 μm wide beam of deuterons ^[4].

It seems that the radiation effect in tissue is dependent not only on the dose but also on the volume exposed, i.e., the smaller the volume, the greater the tolerance.

Synchrotron X-rays achieve the MRT's effect, due to extraordinarily slight divergence, the possibility to use a monoenergetic, or polyenergetic X-ray beam with higher flux and lower energy. This permits to select the best energy for each application, to reduce the dose to the skin.

The target is exposed to multiple quasi-parallel slices of radiation some tens of micrometres, approximately about 25 – 50 μm , spaced 400 – 500 μm centre-to-centre, at kilo voltage energy.

The micro planar beams are produced by a multi-slit collimator, which cuts horizontally (in few cases vertically) microscopic beam sectors from a wiggler-generated fan beam. As the fan beam has a small vertical dimension, larger treatment fields are generated by moving the patient vertically through this field using a computer-guided platform. The speed of vertical translation of the platform, the vertical dimension of the beam, and the incident dose rate are the principal determinants of the dose to tissues directly traversed by microbeams ^[5].

Therefore, synchrotron light segmented into lattice of narrow, quasi-parallel, micro planar beams delivered in a single treatment session in a scanning mode. The very high in-beam peak dose zones are separated by very low-dose valley regions. These “peaks” dose is orders of magnitude greater, about 100 Gy, than those normally delivered in conventional RT.

This extremely high X-ray dose must be delivered at very high dose rates, within a very narrow time window, to prevent blurring of the micro beam tracks due to organ motion, so that the irradiation of an entire organ can be performed in a fraction of a second.

At the moment, the 6-GeV synchrotron ring at ESRF (European Synchrotron Radiation Facility) in Grenoble, is the only in Europe that is capable of generating intense X-ray microbeams, having a broad photon energy spectrum and fluence rates ^[6].

On the global point of view, some few facilities have similar characteristic to develop the microbeam technique, like the already mentioned BNL in Upton, Canadian Light Source (CLS) in Saskatoon, and the Australia Synchrotron in Clayton.

1.1. Peak to valley dose.

One of the most important characteristics of MRT is the spatial fractionation of X-ray beam, which involves in a spatially and periodically alternating microscopic dose distribution. Contrary to most concepts used in clinical radiotherapy, dose deposition in MRT follows an inhomogeneous geometric pattern.

This is achieved by an array of quasi-parallel microbeams, generated by insertion of a specially designed collimator into the primary X-ray beam characterized by a high photon flux.

The target is exposed to this multiple quasi-parallel slices of radiation some tens of micrometres wide spaced of several hundred micrometres centre-to-centre. The very high dose zone is called “peak”, the peaks are separated by very low-dose region, called “valley”.

Figure 1 shows a schematic dose profile between two consecutive micro beams.

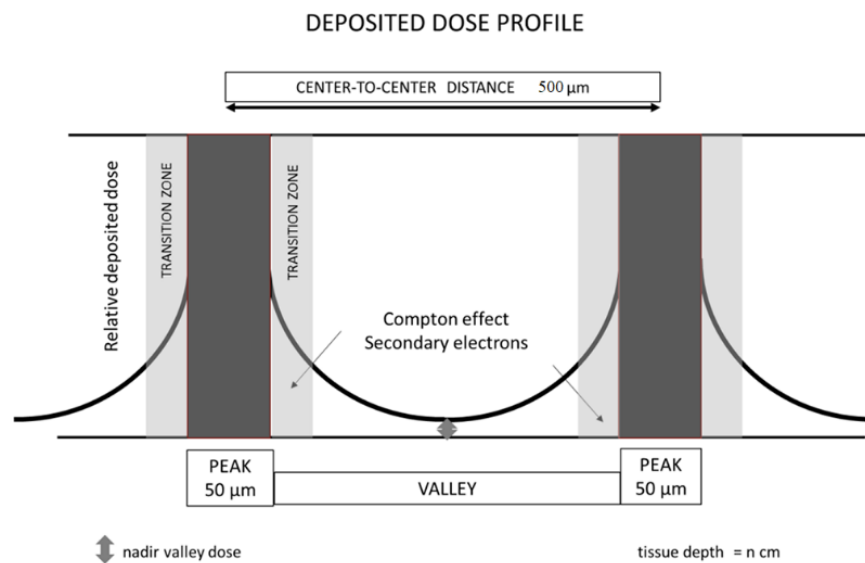


Figure 1: Schematic dose profile in presence of two microbeams, with two characteristic peaks and one valley ^[7].

This dose profile has extremely steep gradients on a microscopic scale. The pattern of peak and valley doses results in the Peak to Valley Dose Ratios (PVDR).

It's very important to estimate PVDR with high accuracy, indeed the radiation effect in tissue is dependent not only on the dose but also on volume exposed, i.e., the smaller the volume, the greater the tolerance.

In the last years, more science activity focuses the attention to improve the Monte Carlo simulation in order to predict this dose profile with high spatial resolution, and research new and more operative method for micro-dosimetry.

The first Monte Carlo calculations in MRT go back to 1992 when Dan Slatkin calculated dose distributions produced inside a human-head phantom. During the last 25 years, most preclinical research has been performed with micro planar beams, due to the ease of manufacturing collimators, which produce planar beams. Early Monte Carlo (MC) simulations benefited from advanced physics models.

Many studies compare several MC codes, including PENELOPE, GEANT and the improved EGSnrc version, in order to determine the most adequate codes for dosimetric studies in MRT due to their advanced low energy electron and photon tracking libraries. A possible improvement to the MC calculations might be the inclusion of the totally reflected photons interacting at grazing angles with the inner surface of the tungsten carbide MSC, which may lead to a small dose contribution of photons from that surface into the valley area. Their contribution can be estimated to be lower than 5% of the calculated valley dose ^[8]. The most important progress and mandatory step to move forward with the proposed veterinary trials was the development of a fast Treatment Planning System (TPS).

The PVDR is a relative value and consequently becomes important only when dose values are converted from the treatment plan to compute the absolute valley dose for the normal tissue, which corresponds to the classical maximum admissible dose value with respect to normal tissue complications. The strong influence of larger field sizes and tighter c-to-c spacing rapidly leads to very small PVDRs as shown in *Figure 2*.

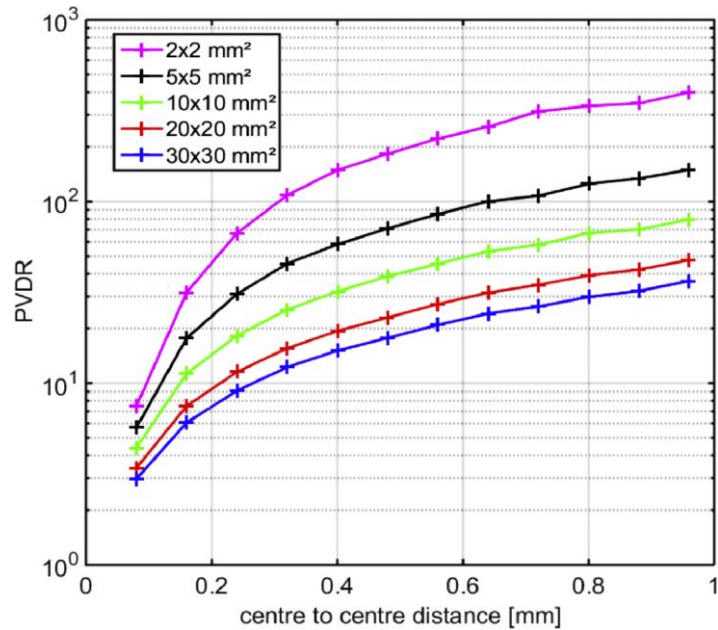


Figure 2: PVDR for different field sizes and centre-to-centre spacing ^[8].

Varies study demonstrated that for microbeam sizes between 25 microns and 75 microns FWHM, the adverse effects or normal tissue complications do only correlate with the valley dose and not with the peak dose. On the other side, preclinical studies show, that a narrow microbeam c-to-c spacing is more effective for tumor growth suppression than a wide microbeam.

MRT-specific effects are related to the surface area between high and low dose regions and the contact surface is certainly instrumental for the repair of heavily irradiated tissues in the peak regions. Most preclinical studies could use small field sizes, with a tight c-to-c spacing and high peak entrance dose values, to achieve a superior tumor control probability (TCP). While the use of larger field sizes and tumor locations at greater depth using relatively low energy photons would oblige to reduce the peak entrance dose values. This has two reasons: minimize the crucial contribution of the valley dose at the tumor and reduce the differential effect on the tumor vasculature from the peak doses for several hundreds of Gy. One possible option to overcome this

problem may be to interspace these microbeams from multiple ports, where larger c-to-c spacing for the normal tissue assures a sufficiently low valley dose and the tighter c-to-c spacing an optimized TCP in the overlap region. A comprehensive MC study focused on comparing different field sizes, target sizes and geometries.

Beginning in the 1990s, there has been a steady increase in the number of publications per year reporting on the technology development and the biological effects of MRT (Figure 3).

New detector systems were developed to satisfy the specific requirements of microdosimetry and Monte Carlo calculation was used in mathematical modelling to understand the challenging basics of MRT dosimetry.

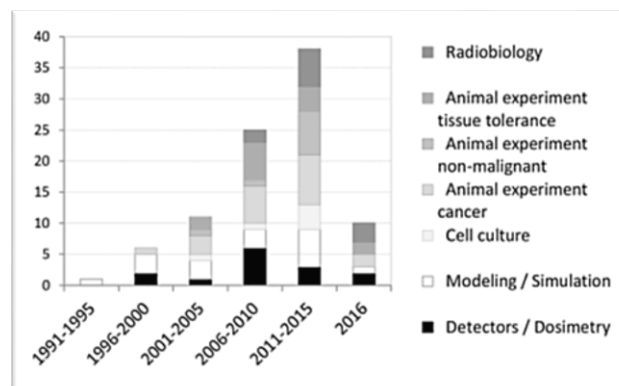


Figure 3: Distribution of publications in the field of MRT in the last twenty-eight years.

1.2. Radiobiology point of view.

The underlying radiobiology of MRT is not well understood. Numerous hypotheses proposed to explain the effectiveness of a treatment, which exposes the tumour to a very steep gradient of ‘peak’ and ‘valley’ doses of radiation.

One of the explanations based on the differential effect of MRT on tumoral and normal tissues' vasculatures. According to this hypothesis, the normal vasculature outside the beams' trajectories is sufficiently well preserved, to allow for a rapid regeneration of blood vessels in the directly irradiated areas (Blattmann et al., 2005).

This hypothesis is based on the assumption that tumours cells need a rich blood supply in order to grow and metastasize (angiogenesis, see *Figure 4*): since the surviving endothelial cells cannot restore the vasculature that was damaged, the entire irradiated segment of tissue starves and dies due also to the lack of oxygenated blood ^[4].

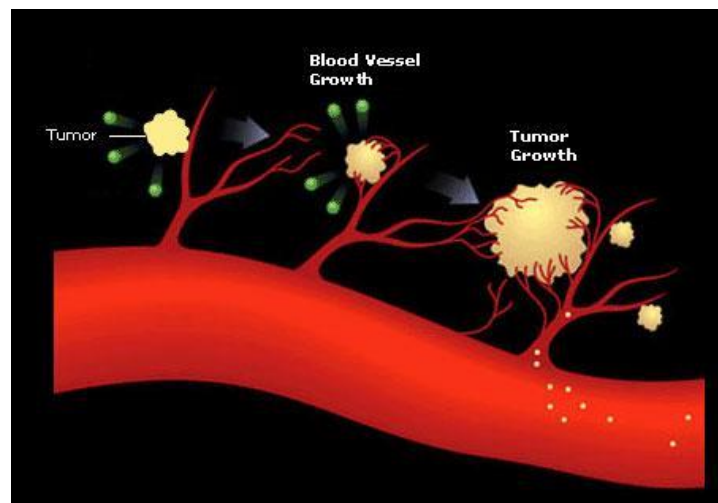


Figure 4: Diagram illustrating the formation of new blood vessels that support tumor growth (angiogenesis) ^[9].

Indeed, there is no intrinsic difference in the radiosensitivity of normal and tumoral cells, but tumoral cells are less able to repair DNA damage. Although this is not true in vitro (tumoral and normal cells grown in culture dishes have the same repair capability), tumoral cells are often oxygen and nutrient deficient. The cells of a tumor divide and proliferate as rapidly as they can, limited only by their own inherited characteristics and the availability of an adequate supply of nutrients. Since a tumor is not an organized

tissue, it tends to outgrow its own blood supply. As the tumor outgrows its vascular system, rapid cell proliferation near capillaries will push other cells into regions remote from a blood supply, where there is an inadequate concentration of oxygen and other nutrients. These cells will die, giving rise to a progressively enlarging necrotic zone.

For the first time in the '60s, the resistance of normal tissues to radiation damage from microbeams of ionizing radiation was observed, during the Zeman and Curtis' studies on the mice, in order to simulate the damage in the human brain caused by energetic cosmic rays during space exploration programs ^[10].

They demonstrated that the mouse-brain cortex can tolerate relatively low doses delivered by a 1-mm-wide beam, while using 25 μm wide microbeams of identical deuterons the tolerance threshold was much higher, on several hundreds of Gray.

Therefore, it was postulated that the vasculature in the microbeam path is rapidly repaired by nominally not irradiated endothelial cells near the track. On the other hand, when the tissue is irradiated with broad beams, the vessels and capillaries may be damaged over areas too large to permit an effective regeneration.

Figure 5 reports histological images of tissues after two different irradiations.

The image on the left side refers to an irradiation with a millimetric beam of relatively low dose (140 Gy), while the right side image shows the effect of irradiation with a narrow microbeam of much higher dose (4000 Gy).

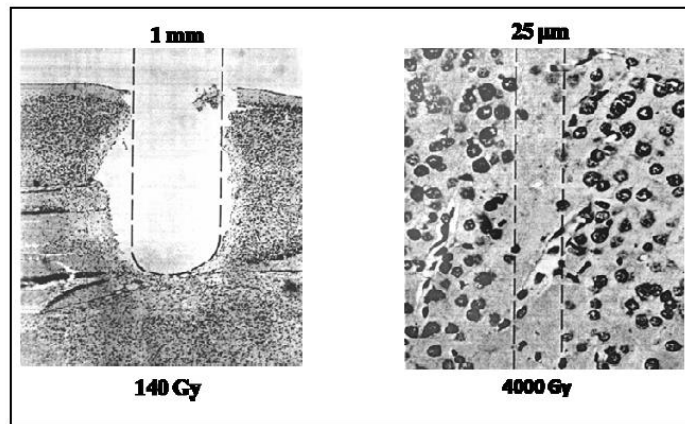


Figure 5: Histological images after irradiation using a millimetric beam (left) and microbeam (right) ^[10].

While deuteron irradiation at a dose of about 140 Gy delivered in a 1 mm wide beam resulted in blood vessel damage and tissue necrosis, the same dose delivered in a 25 μm wide beam caused no damage within a 240 days observation period. Only at and above doses of 4000 Gy, nerve and glial cells in the path of a 25 μm wide beam died within 24 days after irradiation. However, there was no permanent damage to blood vessels and the overall tissue architecture remained intact. In sharp contrast, exposure to a millimetric wide beam caused complete tissue destruction and subsequent cavity formation ^[10].

In contrast with broad-beam irradiations with haemorrhage, wide beams, necrotic regions were seen in the histology already for considerably lower doses. As an explanation of these findings, it was suggested that damaged vasculature in the microbeam track where the so-called “peak dose” is delivered could be repaired by endothelial cells in the vicinity of the track. Since then, several studies have been performed to assess the normal-tissue tolerance to different microbeam doses. In the past decade tumor response to microbeams has been experimentally verified and the

concept of microbeam radiation therapy MRT has been coined. The hypothesis behind MRT, which has now gathered some evidence, is that damaged microvasculature is better repaired in normal tissue than in cancerous tissue.

The basic concept of MRT was developed in the 1980s, but it has not yet been tested in any human clinical trial, even though there is a large number of animal studies demonstrating its marked therapeutic potential with an exceptional normal tissue sparing effect ^[11].

The experiments involved different species as insect, birds, rodents and pigs, that have been revealed an extraordinary tolerance of normal organs and blood vessels exposed to fractionated radiation doses in excess of 100 Gy delivered by an array of microbeams. In 1998, Laissue et al ^[12] were the first to report on the therapeutic efficacy of MRT in a small animal model of malignant brain tumour. Four years later, the first paper on the potential suitability of MRT to treat non-malignant vascular disease was published ^[13]. Soon after therapeutic efficacy of MRT had been established in small animal models, normal tissue tolerance to MRT moved into the focus of interest.

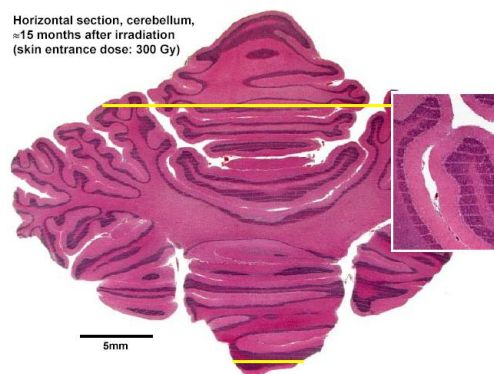


Figure 6: Horizontal section of the cerebellum of a piglet of 15 months after irradiation with a skin entrance dose of 300 Gy. Beam width 27 mm, spacing 210 mm ^[7].

Figure 6 shows a horizontal section of the cerebellum of a piglet of 15 months after irradiation with skin entrance dose of 300 Gy with a beam width of 27 mm and spacing 210 mm. The cells directly in the path of microbeams were destroyed. There was no tissue destruction present, nor were there signs of haemorrhage. The paths of the microbeams appear in the section as thin, white horizontal parallel stripes, which are more easily visible in the insert.

All these studies will further augment understanding of how tumour tissues respond to MRT and serve as an early warning system for unexpected late adverse effects. Considering that the time course of biological events is compressed in domestic and companion animals compared to humans and that the large animal phase I/II trial precedes human clinical trials by several years, one can re-assess and, if necessary, refine the treatment plan for human patients based on the results obtained in these larger animal studies.

Chapter 2: Simulations

A crucial task in the research for MRT is the determination of dose distributions from X-ray microbeams. Indeed, the size of the microbeams makes it difficult to develop a detector with high spatial resolution. Furthermore, the beam used for MRT can be extremely intense, which can cause saturation in the detected signal. This fact limits the available instruments and techniques, which can be used for measurements. Therefore, Monte Carlo simulations play an important role for calculating dose distributions for MRT.

The aim of this work was to determine the radiation doses deposited by X-ray microbeams in various reference materials such as Plexiglas and glandular tissues in a phantom that simulated the patient in prone position.

2.1. Geant4 code

Monte Carlo simulations base on GEANT4 toolkit, which uses the C++ object-oriented programming computer language. The version used in this work is¹² Geant4.10.00 installed on an Ubuntu 16.04 64-bit Linux virtual machine system.

According to the prescriptions provided by the report of AAPM Task Group 195 (2015), The “Option4” PhysicsList was used in GEANT4, for the constructors and instances that consider the physics processes; this model is designed for any applications requiring higher accuracy of electrons and uses the most accurate standard and low-energy models. The production threshold (“range cut”) fixed for the secondary particles is expressed in terms of the distance traveled by the particles in the medium (skin or breast tissue), converted by Geant4 in terms of energy; e.g. the range cuts of 1 mm for photons

and 1 μm for electrons correspond respectively to about 2.79 keV and 0.99 keV in Plexiglas, and 2.55 keV and 0.99 keV in 50% glandular breast tissue. In order to obtain an accurate measure of the dose deposited by the microbeam on the phantom, the physical processes to be implemented must be carefully selected. For photons, the physical processes relevant to the MRT application are the photoelectric and Rayleigh effects, and the Compton scattering. The electron interactions to be considered in MRT MC dosimetry are the elastic scattering and the ionization. The elastic scattering of low-energy electrons generated in the Compton interactions is of particular importance since it determines how far electrons are transported into the valley region.

2.2. Simulation set-up

The MC simulation's output is the 3D dose distribution in a model breast. We scored the energy released by the interaction with primary particles (photons), and secondaries, i.e. electrons. The Geant4 application was based on a previous code developed by A. Sarno from the Medical Physics group, which used the physics list option4. We evaluated the Peak to Valley Dose Ratio (PVDR) in a projection irradiation, as well as the 3D dose distribution in a 360° tomographic irradiation.

The parallel monoenergetic SR beam is fractionated spatially in a number of beamlets by a comb collimator. In the proposed setup, the patient is in prone position and the breast hangs through a hole in the bed and is hosted in a patient-specific ABS plastic holder, as shown in *Figure 7*.

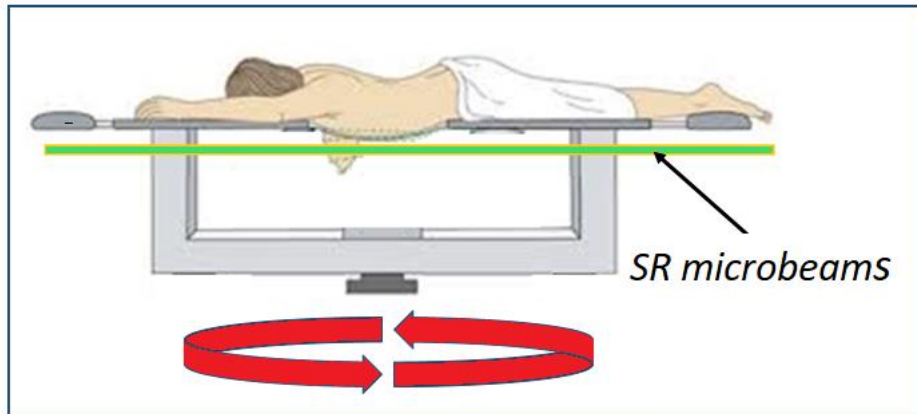


Figure 7: Proposed setup for breast SR radiotherapy, with the patient in prone position and the breast through a hole in the bed.

The pendant breast was modelled as a cylindrical phantom of 14 cm diameter, made of a homogeneous mixture of 50% glandular/50% adipose breast tissue. To simplify the text, this material is indicated as G50. Inside the phantom a small cylinder simulates a tumour mass placed in the centre. Some simulations have been made in Plexiglas (PMMA), in order to compare the results with measurements. *Figure 8* shows the geometry used in the simulation and the coordinate reference system.

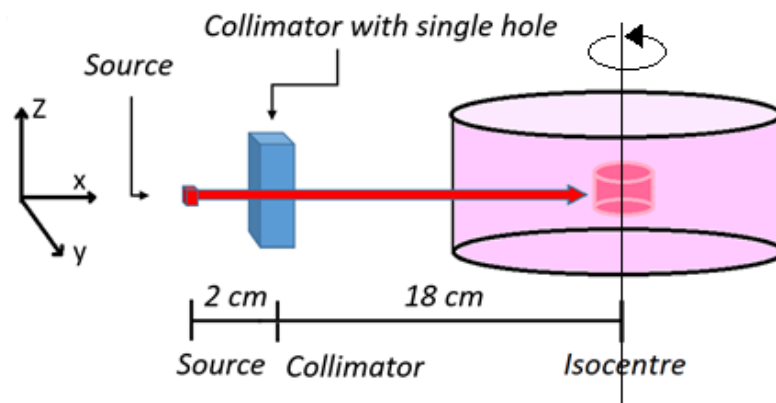


Figure 8: Geometrical scheme of simulation set-up. On the left the coordinate reference system used. In the yz -plane there is the rectangular source, the beam propagates along x -direction towards the phantom. The source is either fixed (projection irradiation) or rotates around an axis passing through the target.

The X-ray source was a rectangular parallel monoenergetic beam, whose rays pass through a tungsten comb collimator (4 mm thick) with slit width 50 μm , along the z-axis and slits separation of 500 μm centre-to-centre. The horizontal slits were perpendicular to the axis of the cylinder, the z-axis of rotation of the proposed setup. The source rotates in a circular or a spiral orbit in a fully tomographic irradiation, for simulating the irradiation of a breast tumour of 1 cm diameter. For reducing the computation time, the vertical collimation of the beam was limited to 1 or 2 mm.

2.3. Collimator

In the GEANT4 simulation's world, the collimator is a tungsten slab inserted in vacuum. This has vertical dimension of 50 μm , along the z-axis, and horizontal dimension of 1 cm. The insertion is repeated with a step of 400 or 500 μm along the z-direction. The select parameters reflect those used for the measurement at CLS.

A physical collimator is under realization via electro-discharge manufacturing at the mechanics shop of this Department of Physics. During the thesis period various steps were completed. *Figure 9* shows the collimator project, the first test in steel INOX (AISI 304), the second test object on a tungsten slab. These had the goal to test the feasibility of the collimator and the minimum slit separation achievable. In *Figure 9.b* it is possible to see that the steel collimator exhibits deformations, when the slit width reduces to 0.3 mm.

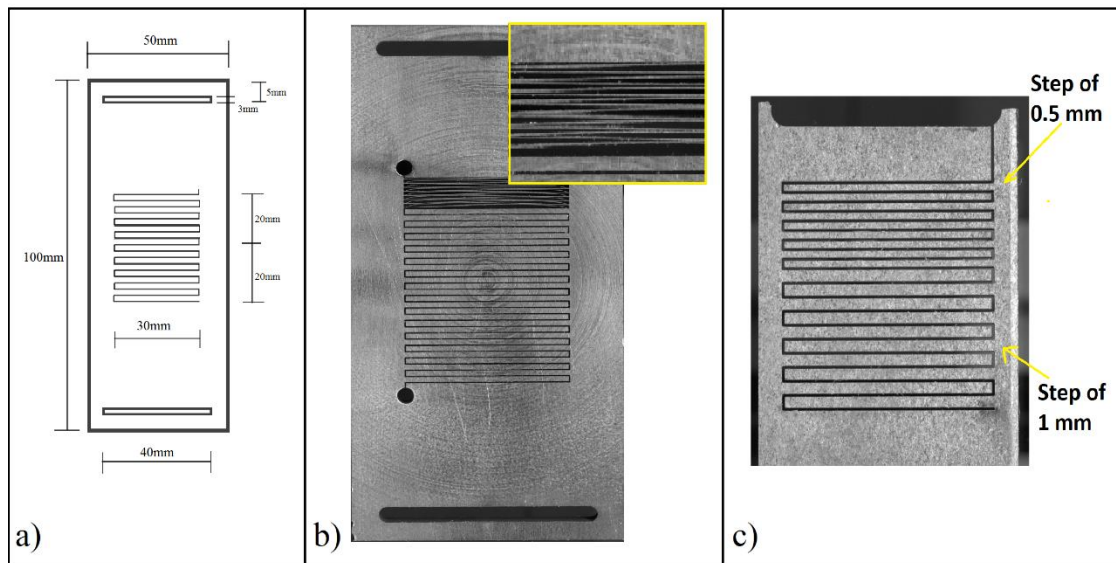


Figure 9: a) collimator project; b) first test on a slab of steel INOX (AISI 304), on the top right material deformation; c) second test on a tungsten slab, with two steps 0.5 mm and 1 mm.

2.4. Single projection

In this section we show the simulations with one single beamlet, the dose profile and the 3D dose distribution in the phantom, simulated with a high spatial resolution in the vertical direction (about 5 μm), for a beam width of 50 μm . Each simulation is monoenergetic, it was repeated at the energy of 80, 100 e 120 keV.

2.4.1. Micro source project

The first problem was how to simulate a micro source. Two approach have been indageted:

- 1) Obtain a micro-source to collimate the beam by interaction with “tungsten slab”, in which have been modelled slits of 50 μm x 1 cm;
- 2) Design a “micro-source” with the dimensions of 50 μm x 1 cm.

The parameters of these simulations are reported in *Table 1*.

Table 1: Simulation’s parameters. The beam width for the micro-source not collimated is of 50 μm .

Phantom		Collimator		Source	
Breast radius, cm	7	Thickness, cm	0.4	Source to isocentre distance, cm	20
Breast height, cm	0.1	Width, cm	2	Beam width, cm	0.01
Mass radius, cm	0.5	Length, cm	2	Beam length, cm	1
Mass height, cm	0.05	Slit width, μm	5		
Slice thickness, μm	5				
Pixel size, cm	0.1				

The phantom material is PMMA. The following data show the dose distribution for a single projection; each has been conducted for a number of primary photon histories equal to 10^8 . In order to estimate the dose contribution with and without the collimator, we run two simulations with the same parameters, but in the first, the beam is modelled as a microbeam by the interaction with the collimator. In the second simulation only the source is present with micrometer dimension along the vertical direction. The simulation output is a stack of tiff images that represents the 3d dose distribution in the phantom. I evaluated the vertical profile in a ROI (Region of Interest) of 1 mm^2 placed centrally at the phantom edge, and the planar profile along the beam direction. For the sake of clarity, the *Figure 10* shows the chose ROIs on a slice used in the case of projection irradiation. The two types of simulations are coincident within 1% (i.e. consistent with the statistical uncertainties in a single simulation run). The same result have been obtained for the simulations at the energy of 80 and 120 keV. Therefore, the presence of the collimation for the source does not change the dose distribution in a relevant way, provided that no beam divergence is present. This permitted to design the source as a microbeam array of beamlets, without the “physical collimator” in the simulation’s

world in order to move the source around the phantom and focus the computing power on other aspect, as the accuracy of the score.

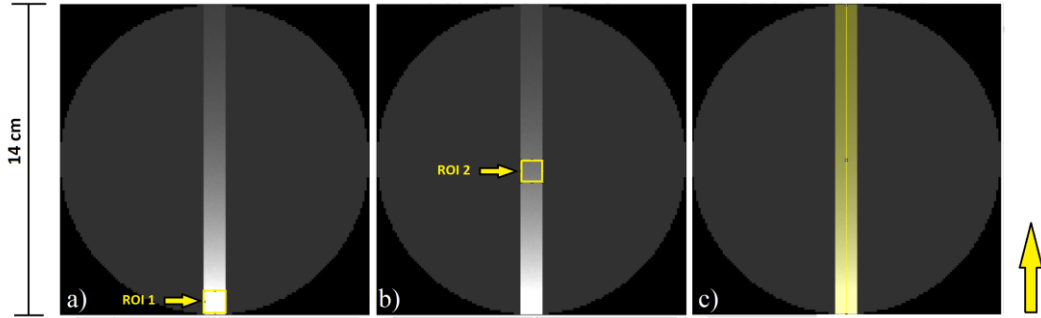


Figure 10: Axial view of a single slice, in yellow a) the ROI_1 is near the phantom's edge, b) the ROI_2 is in the centre at 6.5 cm to the edge, both are of 1 cm²; c) the line used for the planar profile.

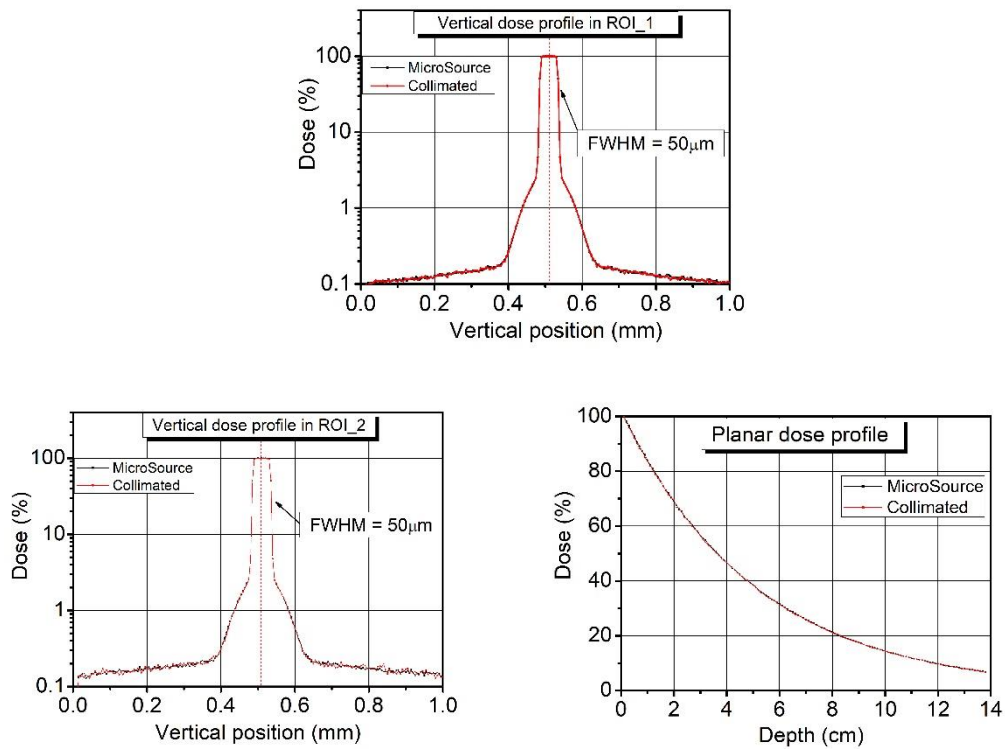


Figure 11: Dose profile at 100 keV in the three ROIs show in the *Figure 10*. The relation between the two simulations is linear, in all three cases, with intercept near to 100%.

2.4.2. Single beamlet

The results on the vertical dose profile for the three energies investigated are shown in *Figure 12*.

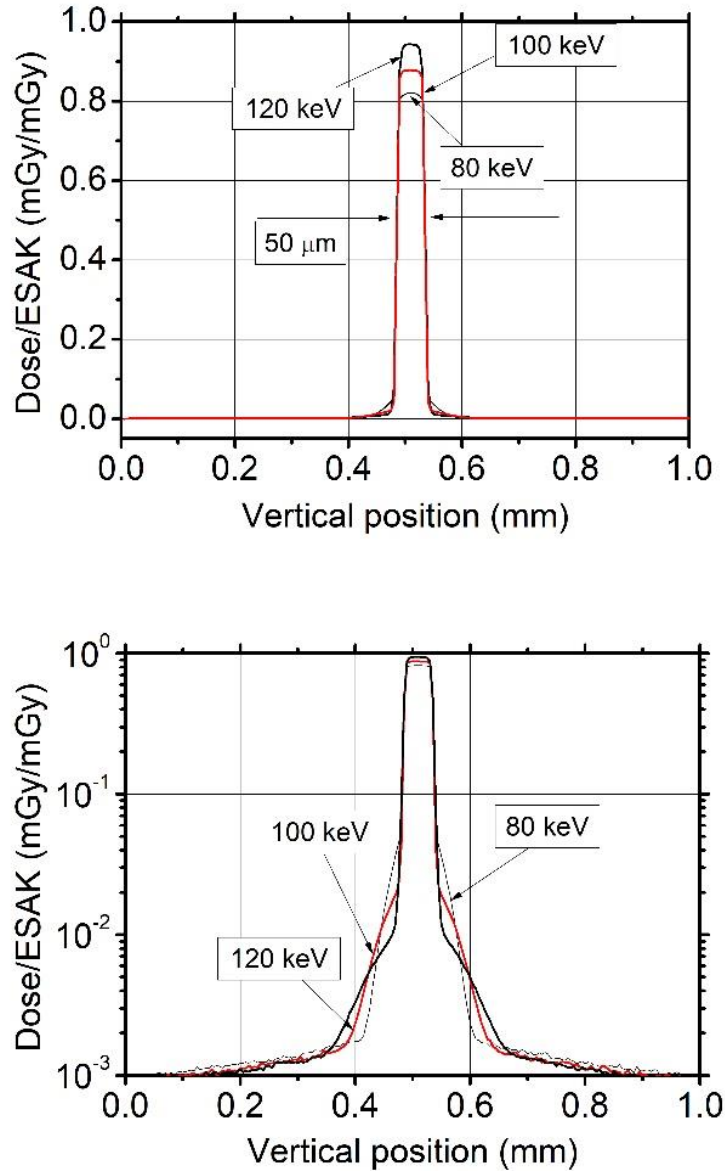


Figure 12 Vertical dose profile for the three energy, (80, 100 and 120 keV) in the ROI_1. Single beamlet of 50 μm width. In the top plot the vertical scale is linear, while on bottom plot the same profile is in a logarithmic vertical scale to put in evidence the low dose tails.

The vertical dose distribution shows two lateral tails due to scatter dose, which were fitted with a Gaussian function, as reported behind, in *Figure 13*. The fitting function

have been evaluated with the commercial software Origin 8 Pro data analysis and graphic package (OriginLab Corporation, Northampton, MA, USA).

The coefficient of determination, R^2 , the FWHM and height for the three energies are listed in *Table 2* and *Table 3*. From these fits it is possible to observe that the FWHM increases as the photon energy increases, while the height of the Gaussian curve decreases. To explain this we must look at the most relevant physical interaction process in the range of our interesting energy: photoelectric and Compton scatter.

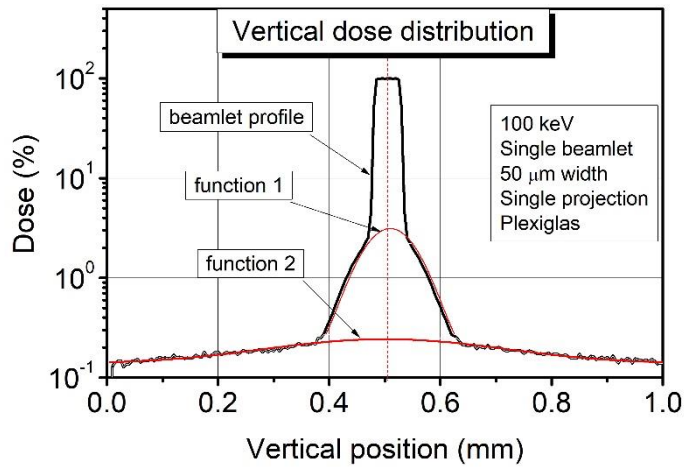


Figure 13: Vertical dose distribution for one beamlet at 100 keV, with the two fit functions in red.

Table 2: Parameters of function 1, for each energy, obtained from the vertical dose distribution.

Function 1	80 keV	100 keV	120 keV
R^2	0.9997	0.9989	0.997
FWHM [mm]	0.076	0.110	0.142
Height [%]	9.4	3.0	1.2

Table 3: Parameters of function 2, for each energy, obtained from the vertical dose distribution.

Function 2	80 keV	100 keV	120 keV
R^2	0.902	0.831	0.917
FWHM [mm]	0.413	0.451	0.505

Height [%]	0.11	0.10	0.08
--------------	------	------	------

From the data report in the two tables, it is possible to observe that the FWHM increases as the photon energy, instead the height of the Gaussian curve decreases. To explain this we must look at the most relevant physical interaction process in the range of our interesting energy: photoelectric and Compton scatter.

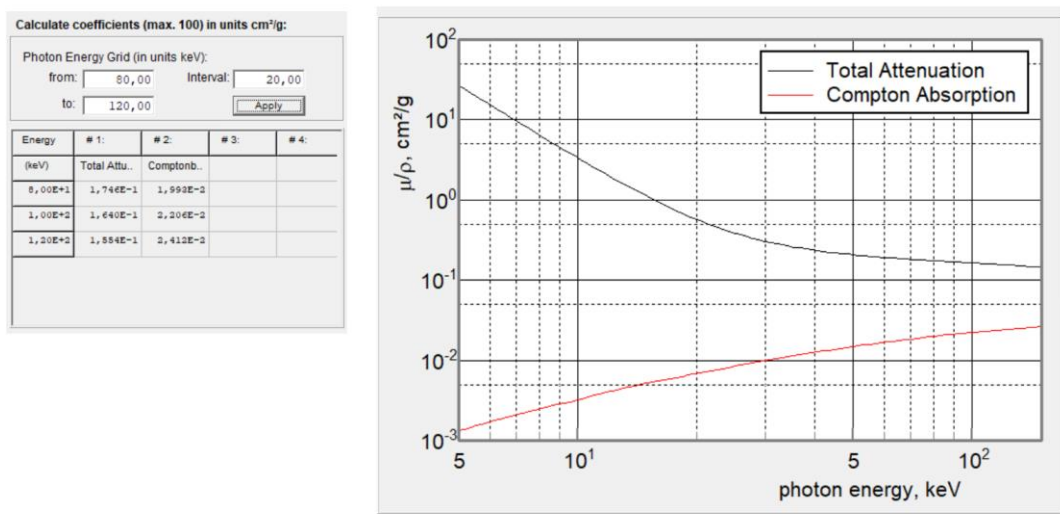


Figure 14 On the left the coefficient value for 80, 100 and 120 keV, on the right the profile from 5 to 150 keV. Both calculated with the software xMuDat.

Figure 14 shows the two coefficients for the PMMA, calculated with the software xMuDat. In the energy range of our interest, the Compton absorption increases, instead, the total attenuation coefficient decreases, but the first is one order of magnitude higher.

2.4.3. Multi beamlets

We now examine the vertical dose profile in presence of multiple beamlets (Figure 16).

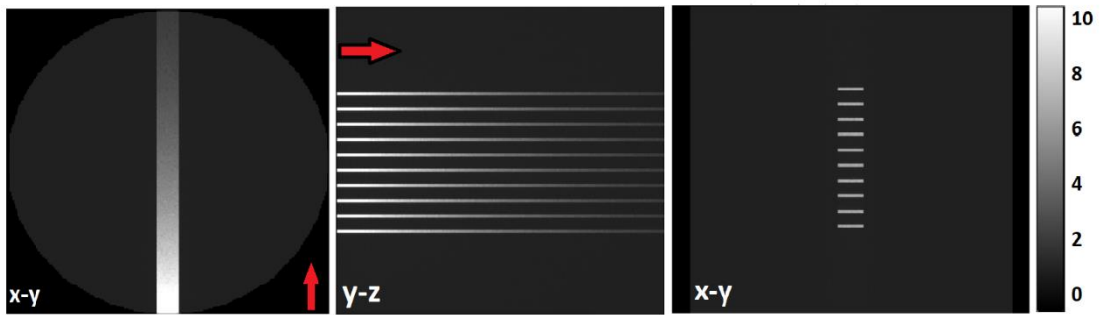
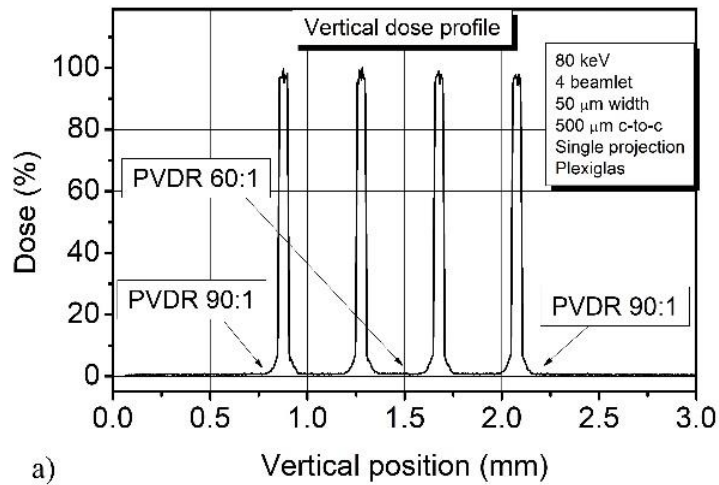


Figure 15 Axial, sagittal and coronal view of the phantom irradiated with ten beamlet. The red arrow indicates the beam direction.

Figure 16 shows that in the presence of an increasing number of vertical beamlets, the PVDR changes in the vertical direction, and at the centre of the beam the PVDR has the lowest value. The PVDR increases by moving toward the extremities of microbeam. As seen in the Figure 13, each beamlet has a scatter dose contribution, that adds up when the microbeam consists of multiple beamlets.



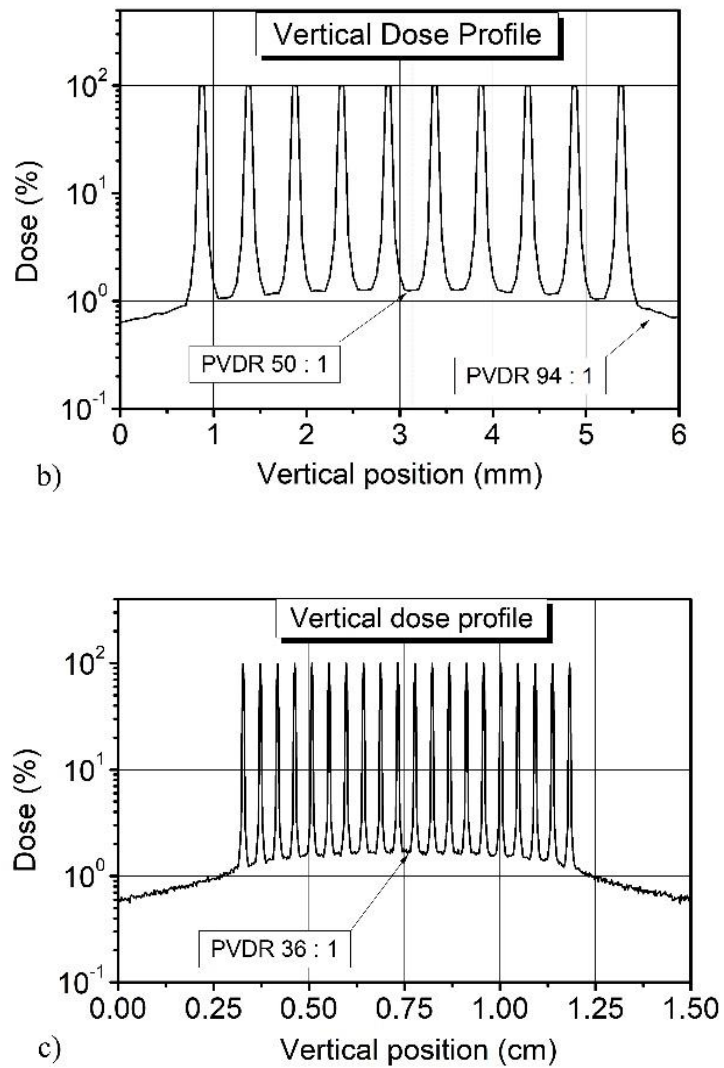


Figure 16 Vertical dose profile obtained simulating a microbeam with a different number of beamlets: four (a), ten (b) and twenty (c).

At the centre of the beam the PVDR has the lower value. The ratio increases by moving toward the end of beam. The difference between the PVDR calculated along the beam grow up with the number of the beamlets. As seen in *Figure 13*, each beamlet has scatter dose contribution, that add up.

2.5. Rotated microbeam

The goal of this thesis work was to investigate the use of microbeam for breast cancer, by rotating the patient bed. In the simulation's world, the geometry is fixed and the source moves on a circular orbit around the phantom simulating the pendant breast, as shown in *Figure 17*.

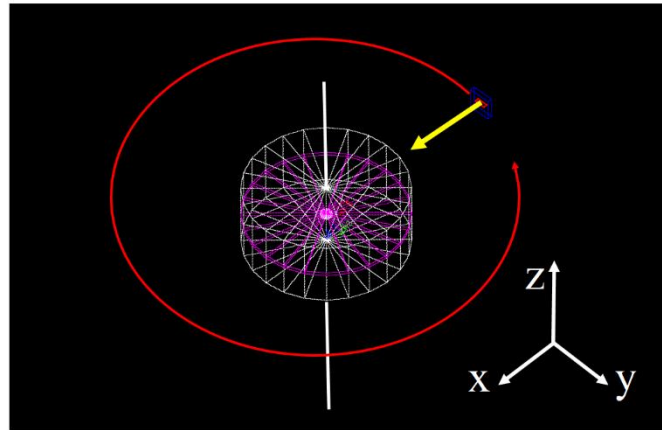


Figure 17 The source, in red, moves around the phantom, along a circular orbit. The rotation axis is in white. It coincides with the z-axis.

The analysis is the same made in the case of single projection. I investigated the distribution dose along the vertical direction (z-axis), for one and four beamlets in Plexiglas, rotating the source around the phantom in order to obtain 360 irradiations, with a step of 1° . In addition, we studied the radial dose distribution, in the transverse plane (xy). The simulation parameters are the same reported in *Table 1*. The total number of primary photon histories is $360 \cdot 10^6$. The ROI used in the analysis are reported in *Figure 18*.

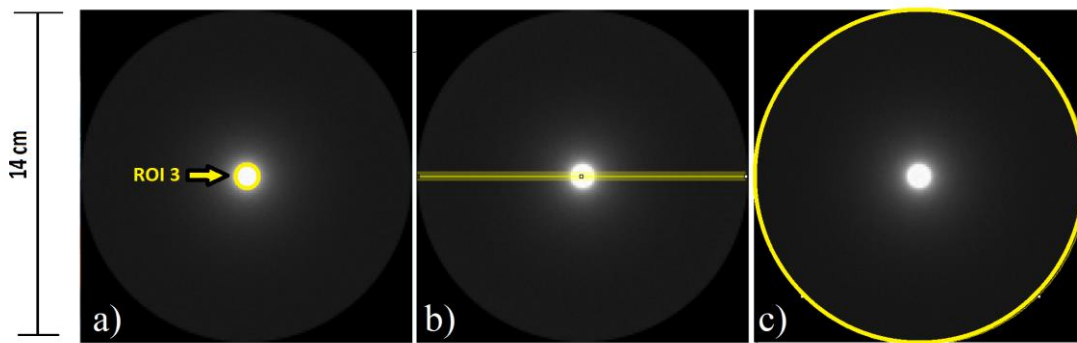


Figure 18 Axial view of a single slice, in yellow a) the ROI_3 is a circle of 1 cm diameter put at the phantom centre; b) the line used for the planar profile and c) the circle with diameter of 14 cm used for the radial profiles.

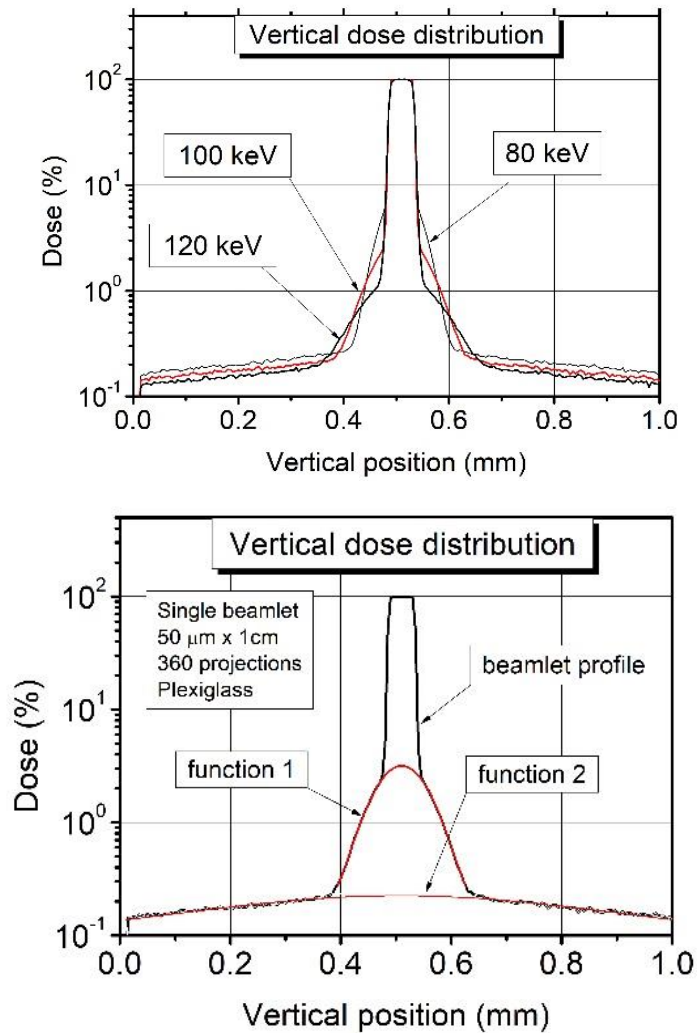


Figure 19 On the left there is vertical dose profile for the three energy (80, 100 and 120 keV) in the ROI_3. On the right is vertical dose distribution for a beamlet at 100 keV, with the two Gaussian fits for the tails of the dose distribution.

The study of vertical dose distributions shows again two Gaussian- shaped tails below the principal peak. The fit parameterises are reported in *Table 4* and *Table 5*.

Table 4 Parameters of function 1 for rotated microbeam on 360°, with one beamlet.

Function 1	80 keV	100 keV	120 keV
R ²	0.999	0.999	0.999
FWHM [mm]	0.076	0.110	0.145
Height [%]	9.4	3.0	1.2

Table 5: Parameters of function 2 for rotated microbeam on 360°, with one beamlet.

Function 2	80 keV	100 keV	120 keV
R ²	0.962	0.942	0.927
FWHM [mm]	0.47	0.48	0.44
Height [%]	0.11	0.095	0.09

As in the single projection study, the dose absorbed outside the track of primary beam, can be attributed to the Compton scatter and the production of secondary electrons. At 80 keV, this is absorbed most near the beam centre than at 120 keV, where the Gaussian curve has the highest value of FWHM and the lower for the height.

On the other hand, when comparing the radial dose distributions at different energies, no significant difference can be found, as shown in *Figure 20*. For all energies the dose drops below 17% at a distance of 2 cm from the central axis of the phantom, and below 10% at 6 cm from the axis (i.e. at 1 cm from the surface). The radial dose distribution with four beamlets has exactly the same profile, as shown in *Figure 20*.

Anyway, in the orthogonal direction (on xy plane) the distribution of the dose is clearly different. Indeed, the orthogonal beam direction is not on micro magnitude, but it is 1 cm wide.

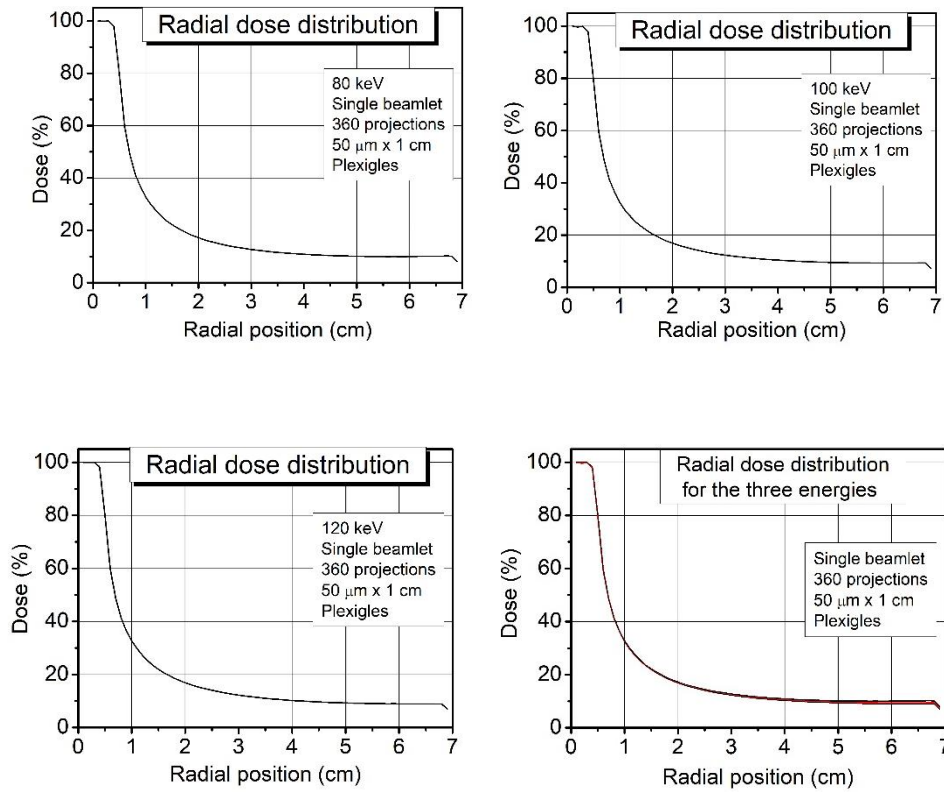


Figure 20: The radial dose distribution for 80, 100 and 120 keV on the central slice. The last plot on the right shows the comparison between the three plots.

For any energy, the dose drop below the 17 % at distance of 2 cm from the beam centre, and below the 10% at 6 cm. From these data, we derived that for a tumour positioned at the phantom centre, the tumour-to-skin dose ratio would be about 9% of the dose delivery to the tumour. It is true for 80, 100 and 120 keV photon energy.

In the previous studies, see Di Lillo et al. 2017 ^[2], with the beam dimension on millimetre, this value is higher, 14% at 60 keV.

This difference is due to a small contribution of lateral scatter to the dose, as a result of beam micro-dimension.

The radial dose distribution with four beamlets exhibits exactly the same profile, as shown in *Figure 21*.

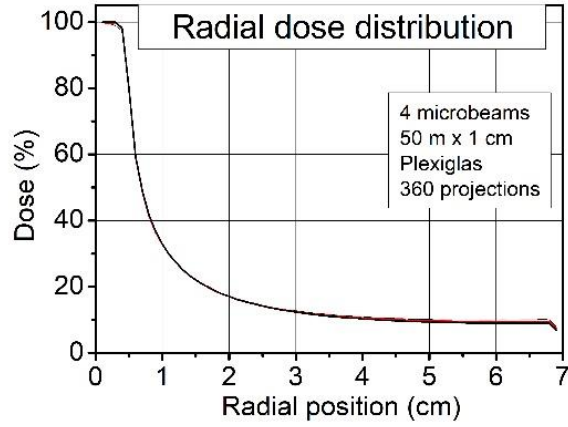


Figure 21 Overlapping of the dose distribution for 80, 100 e 120 keV.

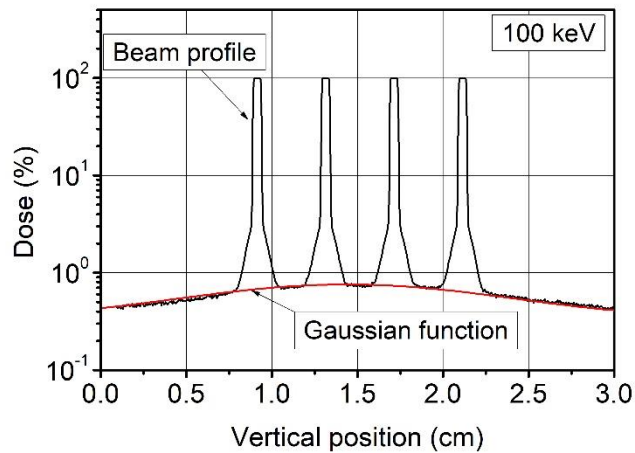


Figure 22 Vertical dose distribution at 100 keV, in red the Gaussian function used to evaluate the dose in the valley.

The *Figure 22* shows the Gaussian function obtained fitting the dose in the valley region. I did the same for the other two energies and reported the parameterises behind, in *Table 6*.

Table 6 Gaussian function parameters, for dose distribution archived by rotated microbeam on 360°, with four beamlets of 50 µm width, in Plexiglas phantom.

	80 keV	100 keV	120 keV
R^2	0.915	0.963	0.950
FWHM [mm]	2.02	1.88	1.83
Height [%]	0.52	0.41	0.37

2.5.1. Different rotational axis

We have seen that for a tumour positioned in the centre of the phantom the dose delivery to the skin is about the 9%. Moving rotational axis of the source, to irradiate a lateral tumour mass, the skin-dose decrease about the 4% (*Figure 24*).

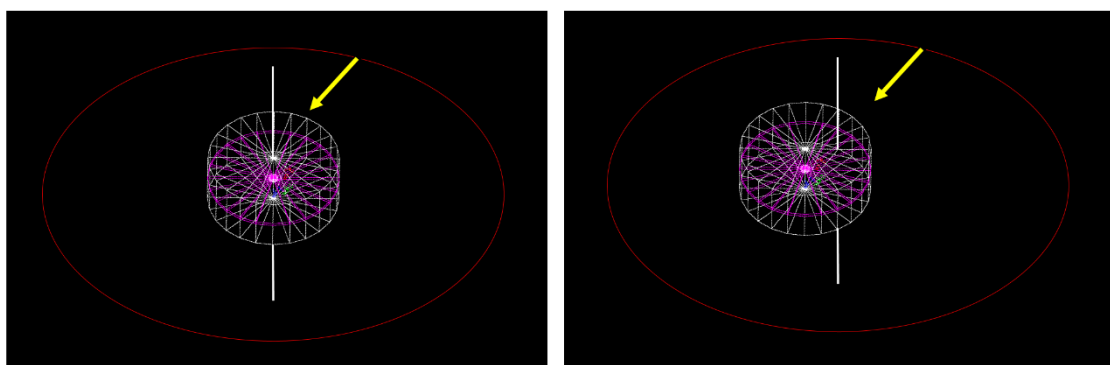


Figure 23 The two rotational source trajectories. On the left, the rotational axis (in white) coincides with the vertical axis of the phantom. On the right, they are distant 35 mm.

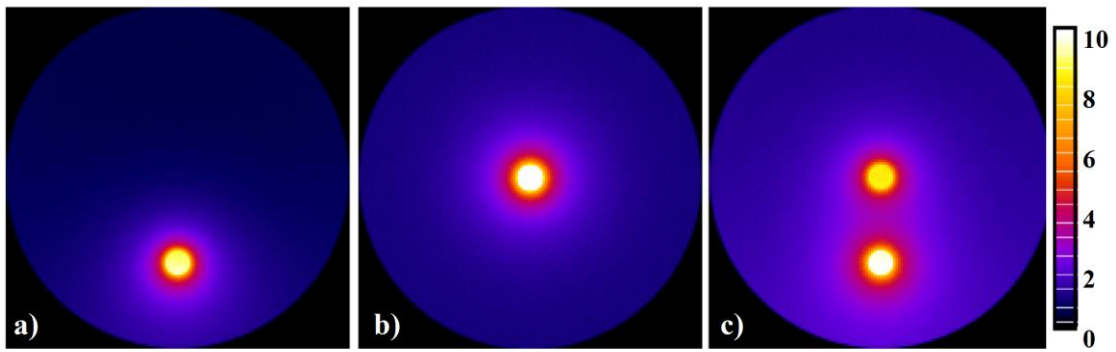


Figure 24 Central slice axial view of the phantom irradiated with rotational microbeam, where a) the rotational axis is moved of 35 mm from the phantom centre, b) the two axis coincides, c) the sum of both. The false colour scale represents increasing percentage dose values (from black to white).

Figure 25 reports the radial dose profile when the rotational axis coincides with phantom centre and which it is shifted of 35 mm.

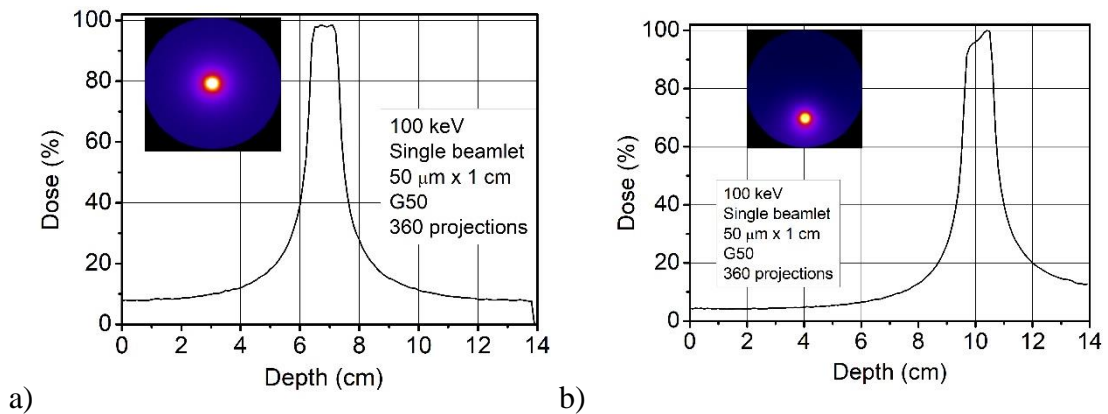


Figure 25 Line dose profile: a) for a central tumor mass, b) for a lateral tumor mass, at 35mm from the centre.

To understand the difference of the peak profile in *Figure 25* I compared the planar dose distribution for a microbeam 14 cm wide, in the orthogonal direction. The results are reported in *Figure 27*.

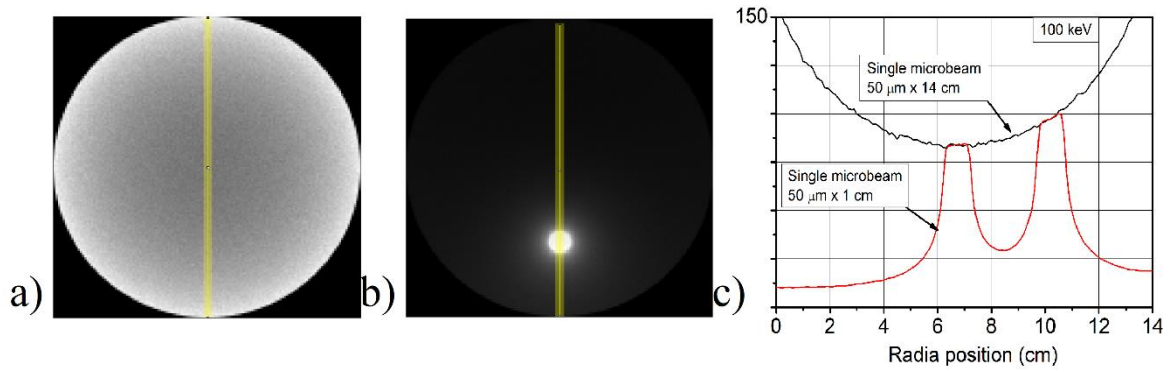


Figure 26 Central slice axial view for phantom irradiated with horizontal beam collimation of 14 cm and rotation around central axis (a), and collimation of 1 cm and rotation around axis shifted of 35mm from the centre (b). Overlapping of the dose distribution for the different collimation.

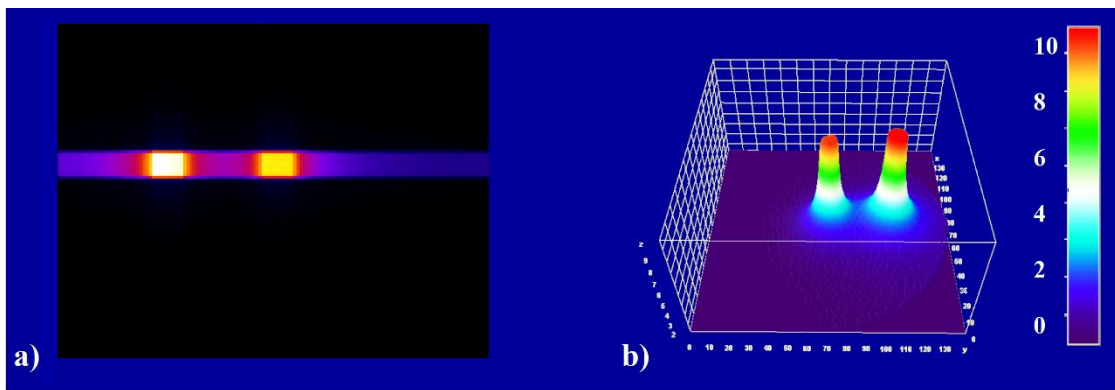


Figure 27 Irradiation of two mass. In a) line dose distribution in coronal view of the phantom, in b) line dose profiles evaluated in terms of percentage of maximum dose. The false colour scale represents increasing percentage dose values (from violet for 0%, to red for 100%).

2.6. Study of the vertical divergence beam

In this section, we show the results of a series of simulations made in order to estimate the effect of a beam divergence in the microbeam width (vertical direction). The simulations refer to a monochromatic beam with different vertical divergence angles, of 0.1, 1 e 10 mrad, respectively. *Figure 28* shows the ROI in the dose map near to the beam entrance, where the dose comparison was made. The phantom was a homogeneous

mixture of 50% glandular/50% adipose breast tissue (G50), irradiated with a single microbeam, $50\mu\text{m} \times 1\text{cm}$ at 100 keV. *Table 7* reports all the specific of simulations.

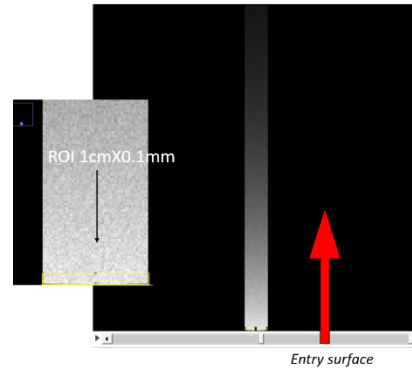


Figure 28: Axial view of a single slice. In evidence on the left the ROI used for the analysis. The red arrow indicates the beam direction.

Table 7: Simulation's parameters.

Phantom	cm	Collimator	cm	Source	cm
Breast radius, cm	7	Thickness, cm	0.4	Source to isocentre distance, cm	20
Breast height, cm	0.2	Width, cm	2	Source to collimator distance, cm	18
Slice thickness, μm	5	Length, cm	2	Beam width, μm	100
Pixel size, μm	200	Slit width, μm	5	Beam length, cm	1

Figure 29 shows the dose profile in the phantom for each divergent microbeam. The profile analyses give us the peak height in term of the dose and the FWHM the beamlet width in the phantom. *Table 8* reports this two values for each divergent angle.

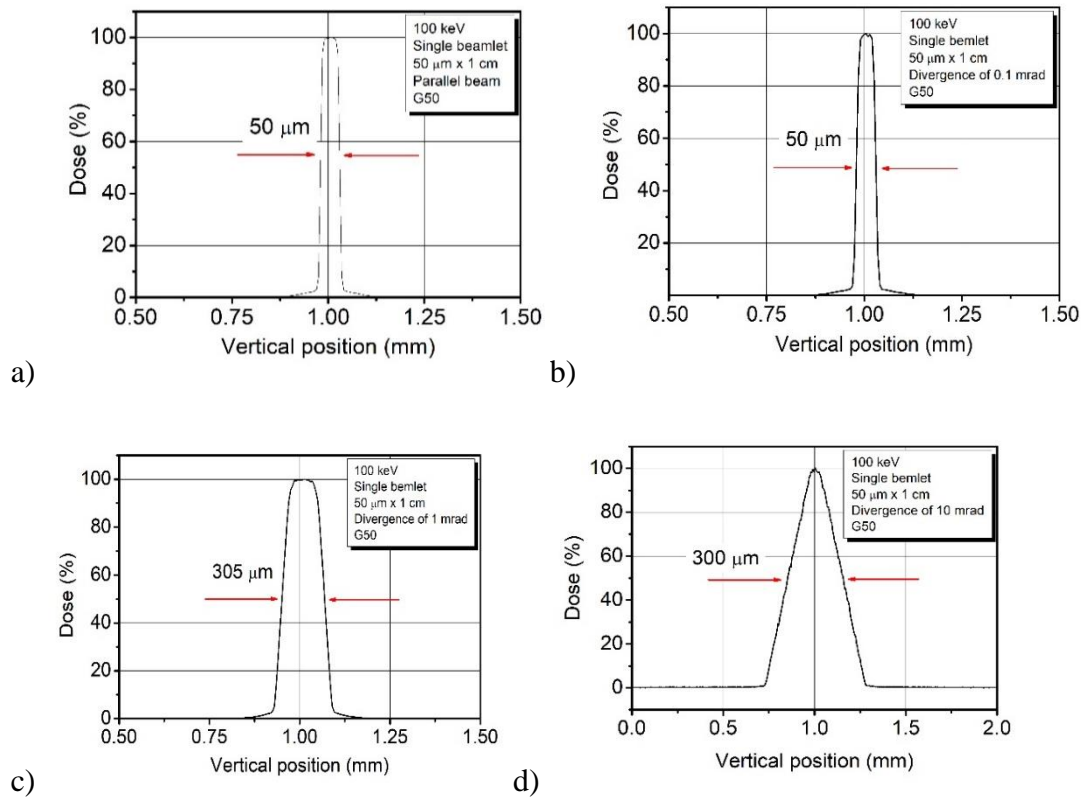


Figure 29: Vertical dose profile for a single beamlet with difference vertical divergence. In order the plots show the dose distribution for parallel beam (a) and beam with divergence of 0.1 mrad (b), 1 mrad (c) and 10 mrad (d).

Table 8: Dose peak values and FWHM for the microbeam with a divergent source.

Divergence [mrad]	Peak Dose [10^{-11} Gy]	FWHM [μm]
0	7.4	50
0.1	7.3	50
1	3.0	120
10	0.3	300

Influence of the additional divergent on the beamlet width is demonstrated by the increasing FWHM values (Table 8).

So the goal of microbeam technique is lost, because the profile becomes broader of 240% if the source has a divergence greater than 0.1 mrad.

Chapter 3: Dose measurements

Every Monte Carlo code need a validation through measures, to test the goodness of simulation and measurement.

In this chapter, I present the first measure on a radiochromic film irradiated with MRT done in the medical physics laboratory of our department.

This has been done in order to compare the dose distribution find by simulation and what comes out from analysing of radiochromic films.

These have been irradiated with a synchrotron monochromatic microbeam, at Canadian Light Source (CLS) at beamline of biomedical imaging and therapy (BMIT-ID) 05ID-2.

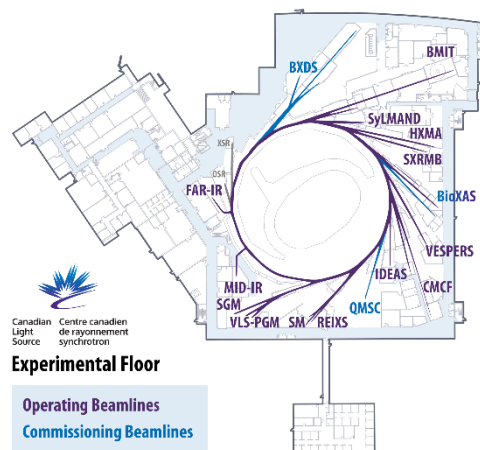


Figure 30 Schematic view of the Canadian Light Source (CLS) synchrotron.

Among the dosimetric 2D detector the radiochromic film offer permanent records of the ionizing dose distribution measured with a high spatial resolutionis. The film contains a dye which changes its colour when exposed to ionising radiation, allowing the level of exposure and beam profile to be characterised.

Film dosimetry was developed and optimized into a powerful tool for radiotherapy treatment verification and quality assurance. Radiochromic films use a radiation-sensitive dye (usually diacetylene monomers organised into microcrystals and embedded in a gelatin binder) to measure the energy of ionizing radiations. Upon irradiation, a solid state polymerization (formation of polydiacetylene dye polymers) takes place and the film adopts a progressively darkening.

Several types of gafchromic film are marketed with differing properties.

For the measurements at the CLS our group used the EBT (External Beam Therapy) GafChromic™ film model, designed to replace silver halide radiographic film for the quality assurance procedures in radiotherapy. The EBT model retained all of the advantages of conventional silver halide film (2D dosimetry, thinness, permanent record, etc.) but without its numerous disadvantages like necessity of chemical development, sensitivity to visible light, strong energy dependence, etc.

Figure 31 shows a simple schema of EBT film layer.

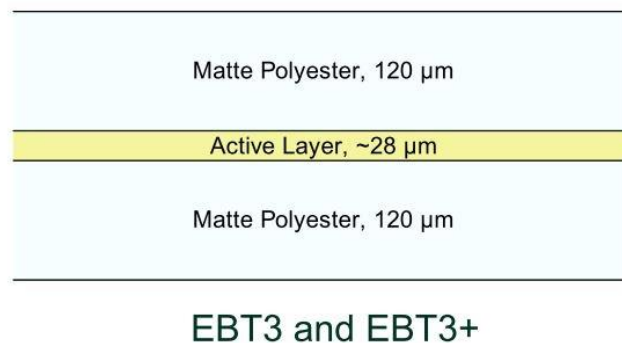


Figure 31 Simply scheme of EBT3 structure layer.

3.1. MRT measurements via EBT3

The GafChromic™ EBT3 films have been irradiated at CLS, by a monochromatic microbeam with photon energy of 80, 100 and 120 keV. The irradiated field was a rectangle of 4.5 mm width and 6.5 mm height. The beam was composed of 16 beamlets of 50 μm , spaced 400 μm c-to-c.

Additional measures have been made with a field of 4 cm^2 , in order to calibrate the radiochromic films.

The films have been scanned with the polarizing microscope AXIOSKOP ZEISS, and the images acquired by the Olympus C-5060 camera, at the non-linear optic at our department, with the collaboration of professor B. Piccirillo.

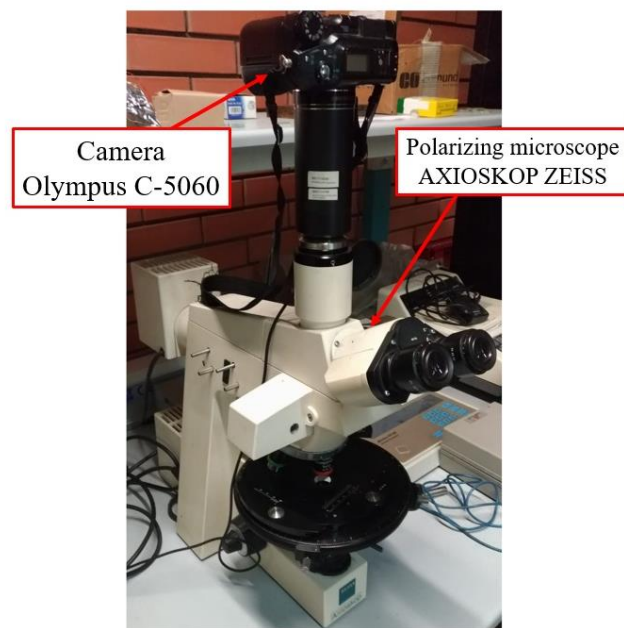


Figure 32: System of reading and acquisition used for the GafChromic™ EBT3 films.

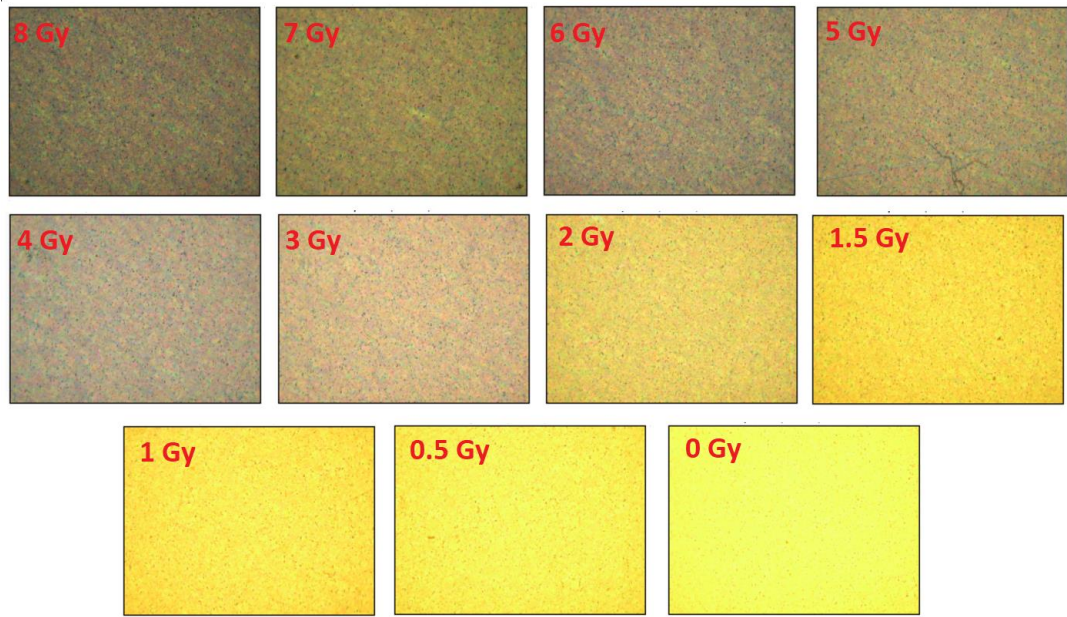


Figure 33: Example of RGB scan images of exposed film pieces in the dose range investigated of 0.5 – 8 Gy, at the monochromatic photon energy of 80keV. The last one is the controller film, which was not irradiated.

The transmission data have been saved as JPEG images, some example are reported in *Figure 33*. Each image have been splitted in RGB channels and analysed with the freeware ImageJ.

A high transmittance value corresponds a high pixel values and a low dose. The better response comes from the green channel for any photon energy. Thus, have been used the calibration curves obtained in this channel for the dose calculation.

The transmittance analyse has been done following “Devic, 2018”^[15], in “single scan mode”, without films scanned before the irradiation.

Devic^[15] has been demonstrated that the use of pre-scanned images to calculate response functions resulted in negligible improvement in dose measurement accuracy.

The transmittance (T) have been calculated as:

$$net\ T = T^{irrad} - T^{unirrad} = \frac{pV^{unirrad} - pV^{irrad}}{2^8} \quad (1)$$

$$\sigma = \sqrt{\frac{\left(\frac{Std_{uniradd}}{2^8}\right)^2 + \left(\frac{Std_{irrad}}{2^8}\right)^2}{2}} \quad (2).$$

Where PV stands for Pixel Value and the term “uniradd” indicates the controller film value.

The calibration curves in the dose range between 0 and 8 Gy, are given in the following figures. They have been calculated with the software OriginPro 8.

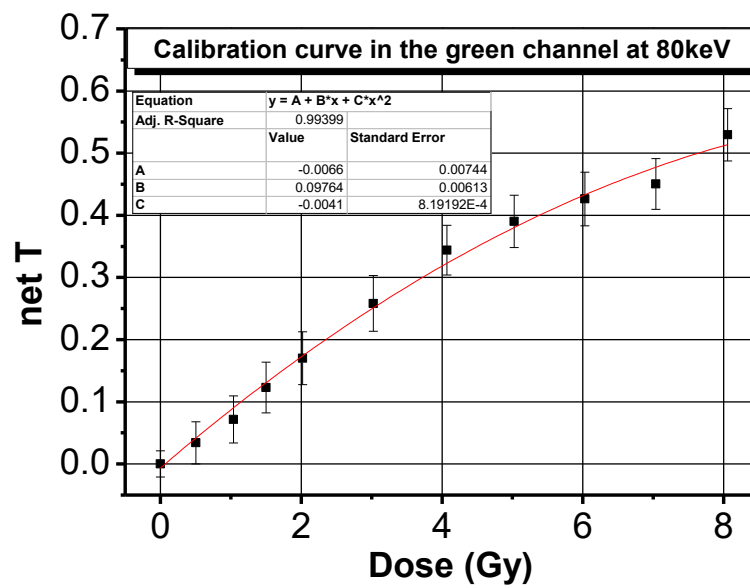


Figure 34: Calibration curve at 80 keV, obtained from the green channel.

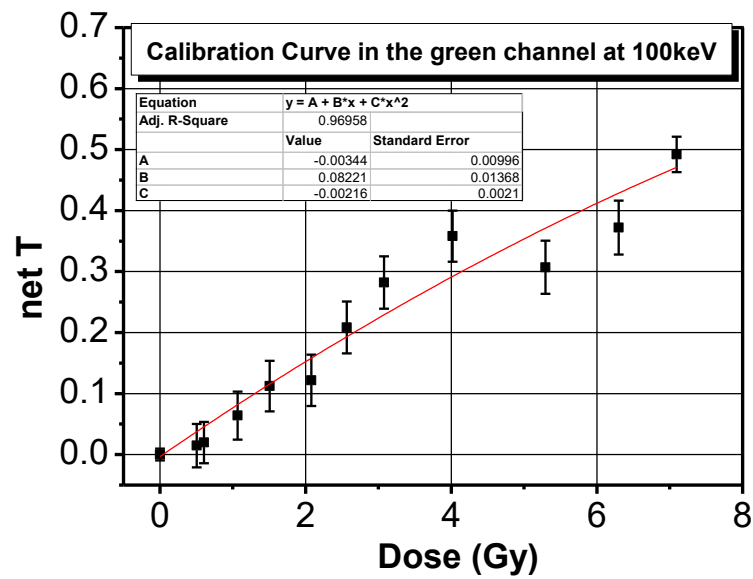


Figure 35: Calibration curve at 100 keV, obtained from the green channel.

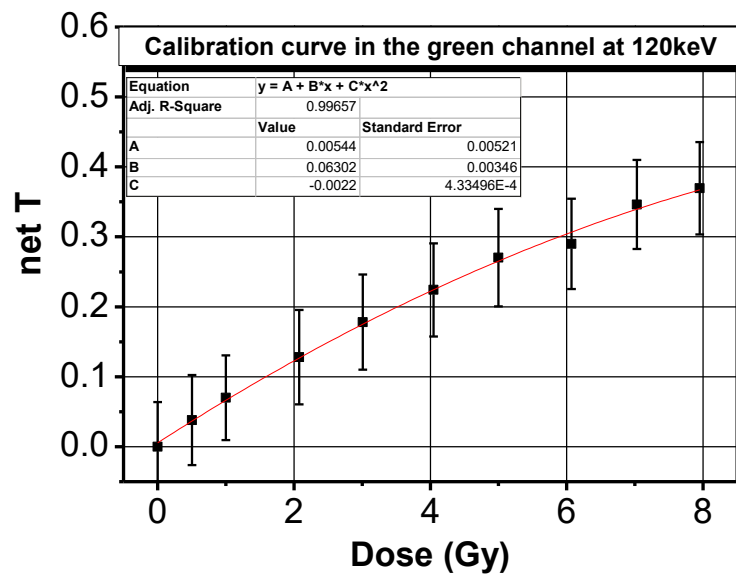


Figure 36 Calibration curve at 120 keV, obtained from the green channel.

A set of films have been irradiated with monochromatic microbeam in rotational mode. The microscope system permit to acquire a field of view of 2.5 x 1.9 mm, so four or five lines are visible in a single scan image. Each represents the dose delivered by a beamlets.

Figure 37 shows an example of dose map obtained by radiochromic film analysed for the investigated photon energies. The image quality decreases for the films irradiated at 100 and 120 keV. For low dose is impossible to distinguish the peak dose from the background, Figure 37.c.

A dose distribution obtained to combine the four images for the film irradiated at 80 keV, is reported in Figure 38 and the calculated dose in Table 9.

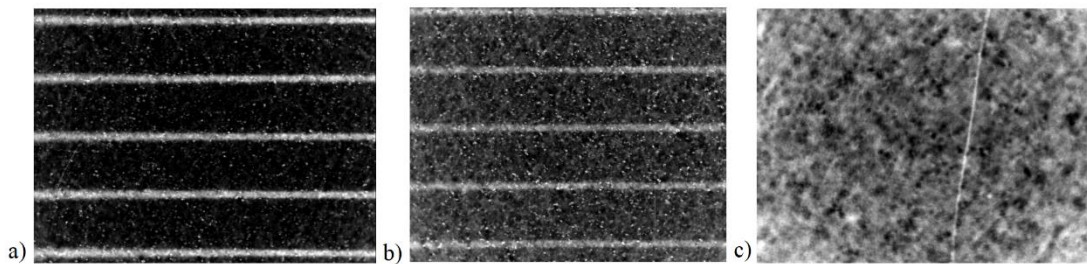


Figure 37: Films irradiated with microbeam after dose calculation by software ImageJ. Dose distribution at 80 keV (a) and 100 keV (b), are visible five beamlets, and four valley. Instead, it is impossible distinguished the slits at 120 keV (c) due to saturation of the image.

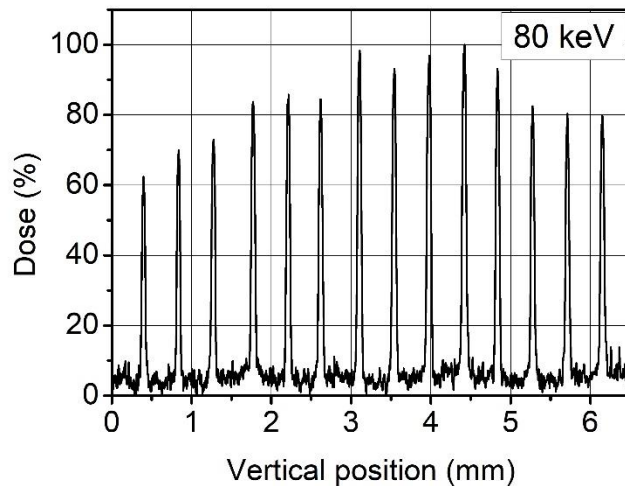


Figure 38 Distribution of dose in percent on all radiated field at 80 keV, obtained by the composed of four images.

Table 9 The mean dose values for peak and valley calculated for films irradiated with rotational microbeam at 80 keV.

	Peak Mean Dose [Gy]	Valley Mean Dose [Gy]
1	1.9±0.8	0.3±0.4
2	2.1±0.8	0.2±0.4
3	2.4±0.8	0.2±0.4
4	3.0±0.8	0.3±0.4
4	2.7±0.8	0.3±0.4
6	2.6±0.8	0.2±0.4
7	2.7±0.8	0.3±0.4
8	3.0±0.9	0.4±0.4
9	3.2±0.9	0.3±0.4
10	3.1±0.9	0.2±0.4
11	3.0±0.8	0.3±0.4
12	3.3±0.8	0.3±0.4
13	3.0±0.9	0.3±0.5
14	2.6±0.9	0.3±0.4
15	2.6±0.8	0.2±0.4
16	2.7±0.7	0.3±0.4

Table 9 reports the mean dose value calculated in the peak and valley region for all the 16 slits. The values in the *valley dose* present a greater standard deviation, due to saturation of the image at low doses.

For the first time, the research group carried out this kind of measurements. Unfortunately, the image quality is limited.

However, it is due micro-dosimetry is today an open question. It is particularly true for MRT, where shall be required a height spatial resolution, on few micrometres.

Conclusion

The Microbeam Radiation Therapy (MRT) is an innovative preclinical technique that uses an array of parallel microbeams of synchrotron-wiggler-generated X-rays. In preclinical trials, it has been shown that MRT can be well tolerated by the normal tissues and can also extend the life span or even cure animals bearing aggressive and radio resistant tumors. MRT is based on the dose-volume effect: normal tissues can tolerate high doses of radiation in small volumes without significant damage. The development of MRT requires reliable estimates of the dose deposition in the peak and valley regions, on a micrometric scale.

In this work, the use of MRT has been investigated for treatment of breast cancer, for the first time. The main objectives consist in calculating dose distributions for MRT with GEANT4 toolkit in order to estimate a crucial parameters associated with the outcome of the treatment, as the *peak-to-valley-dose-ratio* (PVDR). This has been done by considering how simulated dose profiles vary with a series of important parameter using static and rotation source.

The dose distribution delivered in the phantom by a single beamlet has been studied for both of irradiation mode. In the direction where the beam has micro-dimension it shows two Gaussian lateral dose profiles inside the valley region. For monochromatic beams, these may be explained by the contribution of different physical processes at different energies. Dose delivered by secondary particles mainly affect the shape of the these curves. In the other direction, where the beam has millimeter-dimension, the dose profiles show an exponential decrease. In rotation irradiation mode, this produces a

tumour-to-skin dose ratio of about 9% of the dose delivery to the tumour for a central-mass and around the 4% for a lateralles-positioned mass.

Bibliography

1. Siegal RL, Miller KD, Jemal A. Cancer Statistics, 2016. *CA Cancer J Clin* 2016, 66:7-30.
2. F. Di Lillo et al., Towards breast cancer rotational radiotherapy with synchrotron radiation. *Phys. Med.* 2017; 41:20-25.
3. Bouchet A, Bräuer-Krisch E, Prezado Y, El Atifi M, Rogalev L, Le Clec'h C, et al. Better efficacy of synchrotron spatially microfractionated radiation therapy than uniform radiation therapy on glioma. *Int J Radiat Oncol Biol Phys* 2016; 95: 1485–94.
4. J.A. Laissue, N. Lyubimova, H.-P. Wagner, D.W. Archer, D.N. Slatkin, M. Di Michiel, C. Nemoz, M. Renier, E., Bräuer, P.O. Spanne, J.-O. Gebbers, K. Dixon, H.Blattmann, Microbeam radiation therapy, in: H.B. Barber, H. Roehrig (Eds.), *Medical Applications of Penetrating Radiation, Proceedings of SPIE 3770 (1999) 38*.
5. H. Blattmann, J.-O. Gebbers, E. Bräuer-Krisch, A. Bravin, G. Le Duc, W. Burkard, M. Di Michiel, V. Djonov, D.N. Slatkina, J. Stepanek, J.A. Laissue. Applications of synchrotron X-rays to radiotherapy. *Nuclear Instruments and Methods in Physics Research A* 548 (2005) 17–22.
6. M.A. Grotzer, E. Schülke, E.Bräuer-Krisch, J.A. Laissue, Microbeam radiation therapy: Clinical perspectives. *Physica Medica* 31 (2015) 564-567.
7. H. Blattmann, J.-O. Gebbers, E.Bräuer-Krisch, A.Bravin, G. Le Duc, W.Burkard, M. Di Michiel, V. Djonov, D.N. Slatkin, J.Stepanek, J.A.Laissue, Applications of synchrotron X-ray to radiotherapy. *Nuclear Instruments and Methods in Physics Research A* 548 (2005) 17-22.
8. Elke Bräuer-Krisch et al. Medical physics aspects of the synchrotron radiation therapies: Microbeam radiation therapy (MRT) and synchrotron stereotactic radiotherapy (SSRT). *Physica Medica* 31 (2015) 568e583.

9. Jenny Spiga. Monte Carlo simulation of dose distributions for synchrotron Microbeam Radiation Therapy. *PhD thesis, 2005*
10. Zeman W, Curtis HJ, Baker CP. Histopathologic effect of high-energy particle microbeams on the visual cortex of the mouse brain. *Radiat Res 1961; 15:496–514.*
11. Schültke E, Balosso J, Breslin T, Cavaletti G, Djonov V, Esteve F, et al. Microbeam radiation therapy — grid therapy and beyond: a clinical perspective. *Br J Radiol 2017; 90: 20170073.*
12. Laissue JA, Geiser G, Spanne PO, Dilmanian FA, Gebbers JO, Geiser M, et al. Neuropathology of ablation of rat gliosarcomas and contiguous brain tissues using a microplanar beam of synchrotron-wiggler-generated X rays. *Int J Cancer 1998; 78: 654–60.*
13. Dilmanian FA, Kalef-Ezra J, Petersen MJ, Bozios G, Vosswinkel J, Giron F, et al. Could x-ray microbeams inhibit angioplasty-induced restenosis in the rat carotid artery? *Cardiovasc Radiat Med 2003; 4:139–45.*
14. M.A. Grotzer, E. Schültke, E. Braüer-Krisch, J.A. Laissue. Microbeam radiation therapy: Clinical perspectives. *Physica Medica 3, 2015: 564-567*
15. Saad Aldelaijan, Slobodan Devic. Comparison of dose response functions for EBT3 model GafChromic™ film dosimetry system. *Physica Medica 49, 2018: 112-118*

Acknowledgements

Firstly, I would like to express my sincere gratitude to my tutor Prof. Paolo Russo for sparking in me the interest for medical physic, for his patience, motivation, and immense knowledge.

Thanks to PhD Antonio Sarno for his support, knowledge concerning the Monte Carlo method, and helpful comments to this work.

I wish to extend my thanks to prof. G. Mettivier and B. Piccirillo for helpful in acquired and analyse radiochromic images.

Thanks to prof. G. Pepe for his careful and helpful comments to this work.

Many thanks to all research group: Federica Guida, Francesca Buonanno, Francesca Di Lillo, Francesca Di Franco, Giusy Esposito, Marica Masi for all the good and funny moments we shared during these period.